01 Jun 2022

An Impedance Converter-Based Probe Characterization Method for Magnetic Materials' Loss Measurement

Anfeng Huang

Hongseok Kim
Missouri University of Science and Technology, kimhong@mst.edu

Hanyu Zhang

Qiusen He

et. al. For a complete list of authors, see https://scholarsmine.mst.edu/ele_comeng_facwork/4648

Recommended Citation

A. Huang et al., "An Impedance Converter-Based Probe Characterization Method for Magnetic Materials' Loss Measurement," *IEEE Journal of Emerging and Selected Topics in Power Electronics*, vol. 10, no. 3, pp. 3045 - 3054, Institute of Electrical and Electronics Engineers, Jun 2022.
The definitive version is available at https://doi.org/10.1109/JESTPE.2021.3119558

An Impedance Converter-Based Probe Characterization Method for Magnetic Materials' Loss Measurement

Anfeng Huang, *Student Member, IEEE* , Hongseok Kim, *Member, IEEE*, Hanyu Zhang, Qiusen He, David Pommerenke, *Fellow, IEEE*, and Jun Fan, *Fellow, IEEE*

***Abstract*— As an essential component in power applications, magnetic cores and their design play an important role in achieving high efficiency and high power density. Accurate measurement of the core loss is important for inductor and power converter optimization. Loss measurement depends on exactly determining the phase angle between the voltage and the current. However, measurement errors can be introduced due to the discrepancies in propagation delays in the voltage and current sensors. In addition, the propagation delay is frequency-dependent but has a large influence in the MHz range and above. Previously, several methods have been proposed to compensate for this discrepancy, but they are time-consuming and can result in large measurement errors. In this article, a characterization method for core loss based on a vector network analyzer (VNA) and an impedance converter is proposed to accurately measure the phase discrepancies between voltage and current sensors. The proposed method is experimentally verified up to 15 MHz with a three-coil test setup.**

***Index Terms*— Core loss characterization, impedance converter, phase discrepancy, vector network analyzer (VNA).**

I. Introduction

MAGNETIC components (e.g., inductors and transformers) are critical components in power electronics applications [1]–[4]. Due to their high permeability, ferrites are used to reduce the physical dimension of these passive components. However, ferrites are nonlinear. Losses can be influenced by the temperature, frequency, and magnetic flux density [5]–[8]. To optimize the performance of inductors and transformers with respect to loss, size, power density, and thermal characteristics, accurate loss measurements for these magnetic materials are essential.

Among the existing methods, the dual-winding measurement method [9]–[11] is the most widely used as the conduction loss of windings can be excluded from the measurement. However, the accuracy of this method is sensitive to the phase error between the voltage and current measurements. Typically, the main discrepancy is caused by imbalanced propagation delays between probes or the phase shift of a nonideal current sensing resistor. As discussed in [11], the phase shift of a 0.2-Ω sensing resistor with a 1-nH parasitic inductor can reach 8.9° at 5 MHz, and a measurement error of larger than 100% can be generated by this level of phase error.

To eliminate the error caused by the phase discrepancy, several methods exist, including the phase difference cancellation method and the probe characterization method.

The error can be almost neglected if the phase difference between the voltage current and current waveforms is perfectly canceled, which can be achieved with an additional capacitor [9], [10] or inductor [10]. Accurate core loss can be characterized by these techniques; however, perfect phase cancellation can only be achieved at a single frequency, which makes the tuning process burdensome. In addition, due to the nonlinearity of magnetic material, the permeability of the core can change with the excitation level. The compensation reactance needs to be changed with the excitation level even for a single frequency as the inductance value of the inductor can change. The requirement for perfect resonance compensation makes this method time-consuming and cumbersome. An improved partial cancellation method is proposed in [11], which enables accurate core loss characterization without fine-tuning. Although perfect cancellation is not required, different cancellation factors are required for different devices under test (DUTs). Automatic core loss measurement is still challenging for the method.

The simplicity of core loss measurement can be greatly improved if the probes can be rigorously characterized. This avoids a tedious reactance tuning process and allows standardized core loss characterization without changing the compensation parameters A ferrite loss characterization method was implemented with voltage, current probes, and an impedance analyzer [12]. The phase error can be compensated during the calibration process. However, only "THRU" calibration can be applied, which cannot eliminate all the effects of probes and parasitics. Moreover, the characterization process is hard to be applied to modern commercial active probes due to the limitation of the probe-to-instrument interface. Besides,

Manuscript received May 11, 2021; revised August 10, 2021; accepted September 28, 2021. Date of publication October 14, 2021; date of current version June 2, 2022. This work was supported in part by the National Science Foundation under Grant IIP-1916535. Recommended for publication by Associate Editor Katherine A. Kim. *(Corresponding author: Anfeng Huang.)*

Anfeng Huang, Hongseok Kim, Hanyu Zhang, Qiusen He, and Jun Fan are with the Electromagnetic Compatibility (EMC) Laboratory, Missouri University of Science and Technology, Rolla, MO 65409 USA (e-mail: ah4d8@mst.edu; kimhong@mst.edu; hzc5z@mst.edu; qh6g3@mst.edu; jfan@mst.edu).

David Pommerenke is with the Graz University of Technology, 8010 Graz, Austria (e-mail: david.pommerenke@tugraz.at).

Color versions of one or more figures in this article are available at https://doi.org/10.1109/JESTPE.2021.3119558.

Digital Object Identifier 10.1109/JESTPE.2021.3119558

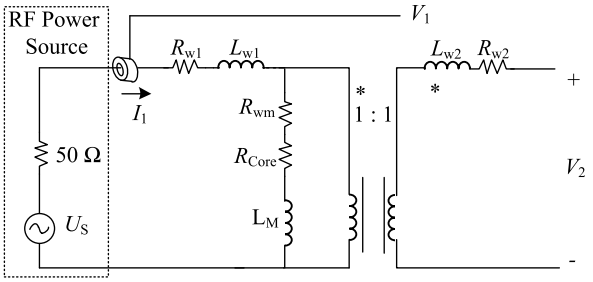

Fig. 1. Equivalent circuit for the dual-winding measurement setup.

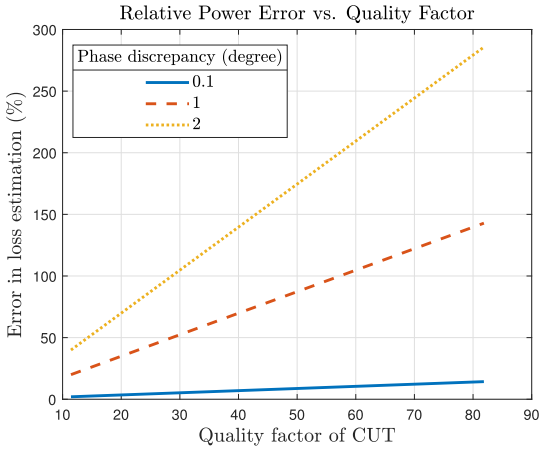

Fig. 2. Error versus Q factor for different phase discrepancy levels.

the method is invalidated when the core sample is operating in the nonlinear region, as impedance analyzers are designed for linear components.

In this article, an impedance converter-based in-house probe is proposed to address these challenges. The wideband phase shift and attenuation of the probe can be characterized by a vector network analyzer (VNA), which provides a constant compensation factor for different measurement configurations. Thus, the core loss can be accurately measured with an ordinary dual-winding measurement setup without extra compensation components. The proposed method is validated by an air-core three-coil system up to 15 MHz. This article is organized as follows. In Section II, the phase discrepancy introduced core loss measurement error is analyzed, and the in-ideal performance of a commercial active probe is demonstrated. The proposed impedance converter-based in-house probe and its characterization method are discussed in Sections II and III. Section IV validates the proposed method for several cores with different materials. In Sections V and VI, the error analysis and conclusion are provided, respectively.

II. Overview of the Dual-Winding Method

A. Sensitivity to Phase Discrepancy

Fig. 1 shows an equivalent circuit for a general dual-winding measurement setup. The DUT carries two windings with identical turn numbers, and the two windings serve exciting and sensing purposes separately. R_{w1}, R_{w2}, L_M, L_{w1}, and L_{w2} correspond to the equivalent series resistances (ESRs) and the magnetizing and leakage inductances of the winding wires. R_{Core} represents the core loss, which includes hysteresis, eddy current, and residual loss in the magnetic material. The mutual resistance due to the proximity effect in the windings should also be considered [13], [14], which is denoted as R_{wm}.

The loss generated by core and mutual-winding resistance can be characterized by measuring the primary winding current I_1 and the open-circuit voltage V_2 of the secondary winding. It can be formulated as

$$\begin{aligned} P_{\text{Mutual}} &= \frac{1}{T}\int_0^T V_2 \cdot I_1 dt \\ &= \frac{1}{T}\int_0^T V_2 \cdot \frac{V_1}{Z_t} dt \end{aligned} \tag{1}$$

where Z_t is the I–V transfer impedance of the current sensor and T denotes the period of the excitation signal. The mutual winding loss R_{wm} can be extracted and canceled, and the core loss can be expressed as

$$P_{\text{Core}} = P_{\text{Mutual}} - \int_0^T I_1^2 R_{\text{wm}}. \tag{2}$$

The phase difference between V_2 and I_1 is close to 90° in a low-loss transformer. Thus, propagation delay between the voltage and current probes is one of the main error sources in ferrite loss characterization. The sensitivity of loss measurement has been well-discussed in [9] and can be formulated as

$$\begin{aligned} P_{\text{error}} &= \tan(\theta) \cdot \Delta\theta \\ &= Q \cdot \Delta\theta \end{aligned} \tag{3}$$

where θ represents the phase difference between the voltage and current waveforms and $\Delta\theta$ is the phase shift discrepancy between the voltage and current sensors. Q is the quality factor of the ferrite core under test (CUT) and is expressed as

$$Q = \frac{\omega L_M}{R_{\text{Core}}}. \tag{4}$$

Fig. 2 shows the error in the loss measurement caused by the phase discrepancy between probes.

The measurement error increases with the quality factor of the CUT in a fixed measurement setup. A phase discrepancy of 1° can produce 100% error for a coil with a Q factor larger than 60, while the Q factor can even reach 80 in real measurement. As a result, the phase discrepancy can generate a large measurement error in the hundreds of kHz range and above. Moreover, the phase shift of a probe is typically brought by the propagation delay of its cable and the internal amplifier, which is larger under a high-frequency range. As an example, a propagation delay of 28 ns generates a 1° phase shift at 100 kHz, and the phase shift is ten times larger, i.e., 10° at 1 MHz. Therefore, it is essential to compensate for the phase discrepancy, especially for high-frequency and low-loss applications.

B. Challenges in Characterization for Commercial Probes

Most electric ferrite characterization methods [10]–[12], [15] were developed based on commercial

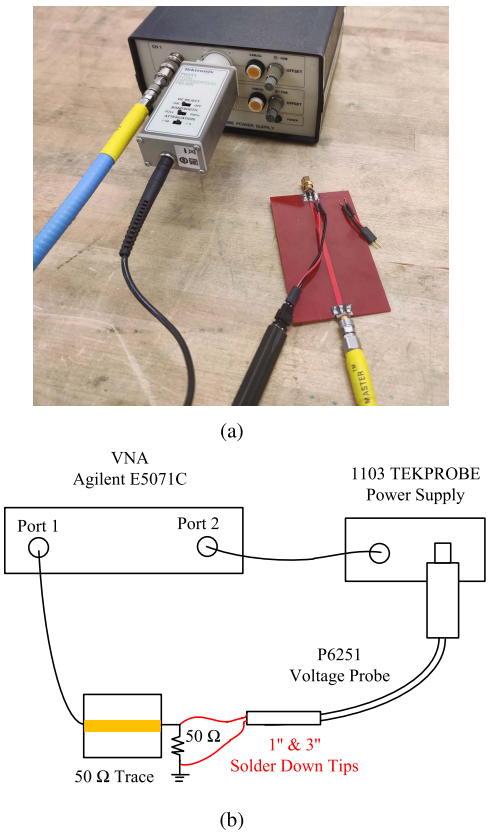

Fig. 3. (a) Photograph of the current probe. (b) Gain and phase of the transfer function for the current probe.

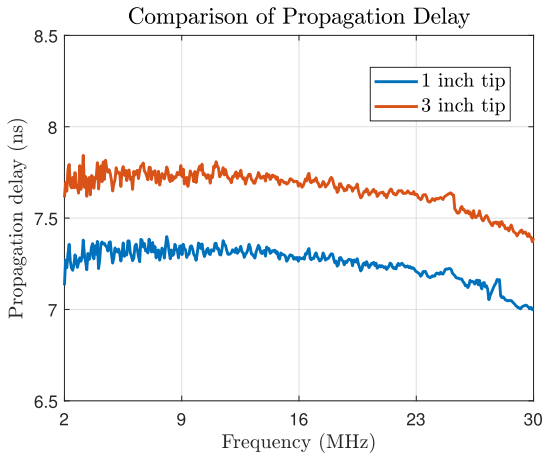

Fig. 4. Measured propagation delays of P6251 with different solder tips.

active probes, which provides high input impedance and consistency of propagation delay between different units. However, the vendors only provide data under limited operating conditions, e.g., the propagation delay from the probe tip to output is provided for a Tektronix P6251 [16]. Extra delay can be introduced by an external probe tip, and the exact value of the delay is not provided.

A VNA is an instrument that measures the wideband network parameters of electric devices and has been widely used for probe characterization [16]. Due to the various

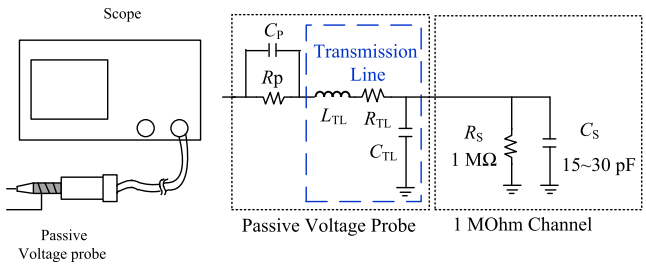

Fig. 5. Equivalent circuit of a probe connected to a 1-MΩ channel.

probe-to-instrument interfaces defined by different manufacturers, using a VNA to measure the electric performance of active probes can be difficult. Fortunately, active probes with a TekProbe interface can be powered by its probe power supply (TekProbe power supply 1103) and connected to any instrument with a 50-Ω input impedance, as shown in Fig. 3. The propagation delay and attenuation of an active voltage probe can be directly extracted from the S_{21} measurement, which is formulated as

$$\text{Attenuation} = 1/\text{mag}(S_{21}) \tag{5}$$

$$T_d = \frac{\Delta\text{Phase}(S_{21})}{\Delta\omega} \tag{6}$$

where ω is the frequency of S_{21}.

The propagation delays and attenuation are measured with the same trace, coax cables, and a 50-Ω terminator, as shown in Fig. 4. A ~300-ps difference in delay is observed, which is brought by the difference in the tip length. The delay due to the probe tip is not provided by the vendor. In addition, the propagation delays are not constant values even in the 2–30-MHz range. Applying delay data provided by the vendor in probe compensation can introduce unacceptable error, especially in high-frequency applications [15]. Even though the measurement accuracy is less sensitive to attenuation error voltage, the nonconstant attenuation will introduce extra error.

In summary, commercial probes cannot provide a constant propagation delay among operating bandwidths. A large measurement error can be generated if the frequency-dependent propagation delay is not captured and compensated.

III. Implementation, Characterization, and Compensation Method for Probes

A probe can be characterized using a VNA, as demonstrated in Section II. An impedance converter is designed, which allows the attachment of high-impedance passive probes to a VNA and gets rid of the limitation of commercial probes. The design considerations for the probing system are also discussed.

A. Implementation and Characterization for Impedance Converter-Based Probe

A passive voltage probe is typically connected to a 1-MΩ input channel of an oscilloscope; the equivalent circuit of both probe and scope is illustrated in Fig. 5.

The passive voltage probe can be modeled as the combination of a parallel *RC* circuit and a transmission line. The probe

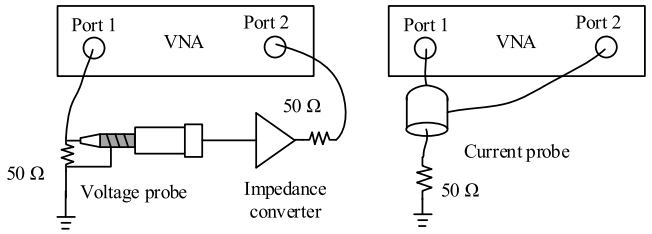

Fig. 6. Characterization setups for voltage probing system and current probe.

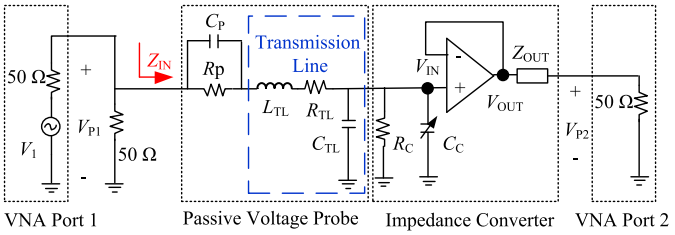

Fig. 7. Equivalent circuit for the voltage probing system characterization setup.

tip resistance R_P is typically 9 MΩ, which gives a 10:1 diving ratio with the scope's 1-MΩ input resistance R_S. At dozens of kHz and above, the same dividing ratio is achieved by the capacitances of the probe tip C_P (typical value: 10 pF), transmission line C_{TL}, and scope channel C_S (typical value: 15∼30 pF) [17].

The impedance converter is then designed to reproduce the input impedance of a 1-MΩ channel of the scope. It consists of an operational amplifier and a parallel RC network. The input–output voltage transfer function of the combined voltage probe and impedance converter $\mathrm{TF_{VP}}$ can be measured by a VNA. The measurement setup and equivalent circuit of the probing system are demonstrated in Figs. 6 and 7, respectively.

As demonstrated in Fig. 7, V_1 is the voltage source generated by port 1 with a 50-Ω source impedance. Port 1 is terminated with a 50-Ω load; therefore, V_{P1} is denoted as the output voltage of port 1 and is measured by the voltage measurement circuit.

To calculate the transfer function of the voltage measurement circuit, the input impedance of the probe needs to be calculated first as

$$Z_{\mathrm{IN}}(\omega) = \left(\frac{1}{j\omega C_P} // R_P\right) + j\omega L_{\mathrm{TL}} + R_{\mathrm{TL}} + \left(\frac{1}{j\omega(C_C + C_{\mathrm{TL}})} // R_C\right). \quad (7)$$

We note that L_{TL} and R_{TL} are in the range of nH and hundreds of ohms and, thus, can be neglected. In addition, in the frequency range of interest (<30 MHz), $Z_{\mathrm{IN}} \gg 50\ \Omega$; therefore, the signal picked up by the voltage probe V_{P1} is given by

$$V_{P1} = V_1 \cdot \frac{(50\ \Omega // Z_P)}{50\ \Omega + (50\ \Omega // Z_P)} \approx \left(\frac{V_1}{2}\right). \quad (8)$$

The output of the voltage probe is connected to the impedance converter, and the input signal of the impedance converter V_{IN} can be easily found as

$$V_{\mathrm{IN}} = V_{P1}\frac{Z_C // Z_{\mathrm{CTL}}}{Z_P} \quad (9)$$

where Z_C and Z_{CTL} are the input impedances of the impedance converter and the parasitic capacitance of the transmission line, respectively,

$$Z_C = R_C // \frac{1}{j\omega C_C} \quad (10)$$

$$Z_{\mathrm{CTL}} = \frac{1}{j\omega C_{\mathrm{CTL}}}. \quad (11)$$

Due to the negative feedback provided by the amplifier, $V_{\mathrm{OUT}} = V_{\mathrm{IN}}$. The voltage V_{P2} induced on port 2 can be written as

$$V_{P2} = V_{\mathrm{OUT}} \cdot \frac{50\ \Omega}{Z_{\mathrm{OUT}} + 50\ \Omega}. \quad (12)$$

The output impedance of the converter is configured to be 50 Ω for impedance matching.

Finally, the transfer function of the combined voltage probe and impedance converter $\mathrm{TF_{VP}}(\omega)$ can be related by the two-port voltages V_{P1} and V_{P2} as

$$\mathrm{TF_{VP}}(\omega) = \frac{V_{P2}}{V_{P1}} = \frac{Z_C // Z_{\mathrm{CTL}}}{2Z_P} = S_{21\mathrm{VP}}. \quad (13)$$

The transfer function $\mathrm{TF_{VP}}$ contains both attenuation and phase information among the whole measurement frequency range.

B. Characterization for Current Probe

The characterization method for the current probe is well known [18], and the measurement setup is depicted in Fig. 6. The current–voltage transfer function of the probe $\mathrm{TF_{CP}}$ at different source frequencies ω can be expressed as

$$\mathrm{TF_{CP}}(\omega) = S_{21\mathrm{CP}} \times 50. \quad (14)$$

C. Measurement Procedure

As the measured phase shift discrepancy is frequency-dependent, the fast Fourier transform (FFT) is applied to the measured time-domain voltage and current waveforms. After compensation is performed in the frequency domain, the loss can be calculated. Then, the inverse FFT (IFFT) is applied for the voltage waveforms, and the compensated peak flux density is obtained. The flowchart of the proposed measurement method is shown in Fig. 8.

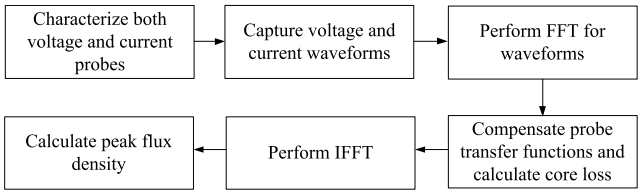

Fig. 8. Flowchart for the proposed method.

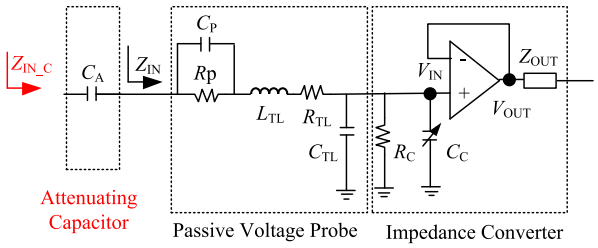

Fig. 9. Equivalent circuit model with the attenuating capacitor.

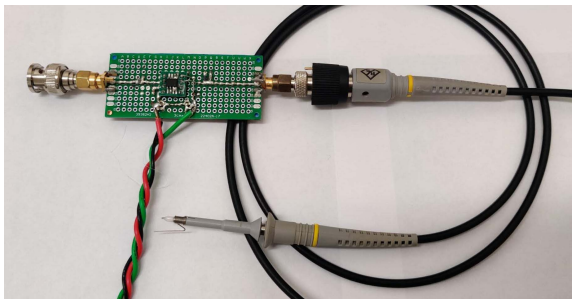

Fig. 10. Prototype of the impedance converter and the passive voltage probe.

D. Design Considerations for the Voltage Probing System

Despite the benefits introduced by the impedance converter, there are still limitations in the designed voltage probing system. First, the high-speed operational amplifiers have a limited voltage output swing (typically less than 10 V), and an extra attenuator is required for high flux measurement cases. Second, the input impedance of passive probes is not sufficient for high-frequency applications [10]. The two issues can be solved by introducing another attenuating capacitor into the probing system, as shown in Fig. 9.

The total input impedance of the probing system $Z_{\mathrm{IN\_C}}$ with the attenuating capacitor C_A is expressed as

$$Z_{\mathrm{IN\_C}} = \frac{1}{j\omega C_A} // Z_{\mathrm{IN}}. \tag{15}$$

In addition, the extra attenuation ratio AR generated by C_A can be formulated as

$$\mathrm{AR} = \frac{Z_{\mathrm{IN}}}{Z_{\mathrm{IN\_C}}}. \tag{16}$$

In summary, both the input impedance and the maximum input voltage of the probing system can be extended with an extra attenuating capacitor.

IV. Characterization of the Voltage Probing System and Current Probe

A. Voltage Probing System

Fig. 10 shows the prototype of the impedance converter and the voltage probe. The impedance converter is built with an operational amplifier (Analog Device ADA4817-1) and a passive probe (R&S RT-ZP10). R_C is configured as 1 MΩ, and C_C is a tunable capacitor whose capacitance value ranges between 1 and 30 pF. This configuration provides an attenuation ratio of 20, i.e., 26 dB.

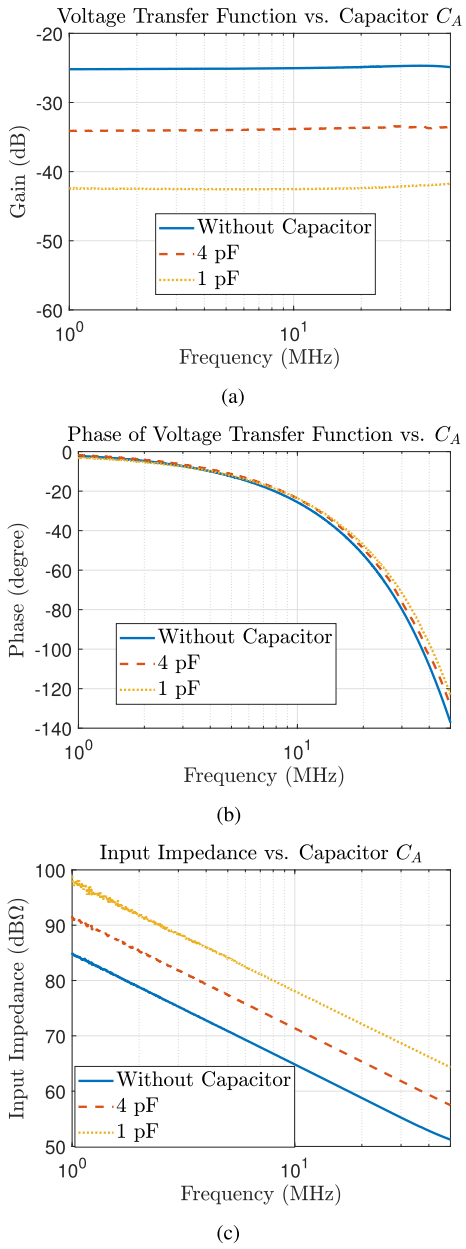

Fig. 11. Influence of C_A on the voltage measurement circuit. (a) Gain of the voltage transfer function. (b) Phase of the voltage transfer function. (c) Input Impedance of the voltage probe.

To verify the proposed equivalent circuit of the voltage probe, the input impedance and the transfer functions are measured for the cases where C_A is not added, $C_A = 4$ pF, and $C_A = 1$ pF. The measurement setup is demonstrated in Fig. 6.

The measured gain and phase values of the voltage transfer function for three cases are shown in Fig. 11(a) and (b), respectively. The calculated gains with a capacitance of 4 and 1 pF are −36 and −46 dB, respectively, which agrees well with the measured results. Smooth voltage transfer functions are obtained up to 50 MHz from the current design and can be extended to a higher frequency with better control of parasitics in the amplifier board.

The input impedance $Z_{\mathrm{IN\_C}}$ also increases with external capacitor C_A, which is verified in Fig. 11(c). The input

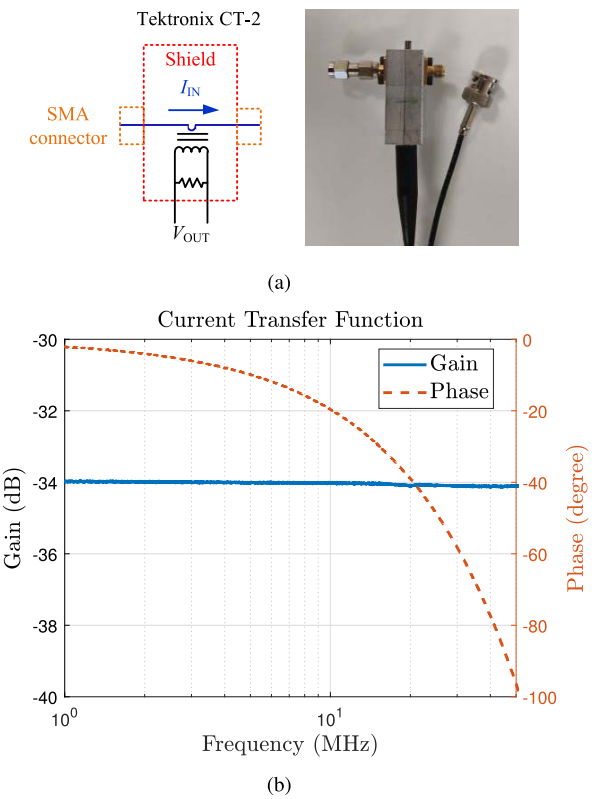

Fig. 12. (a) Photograph of the current probe. (b) Gain and phase of the transfer function for the current probe.

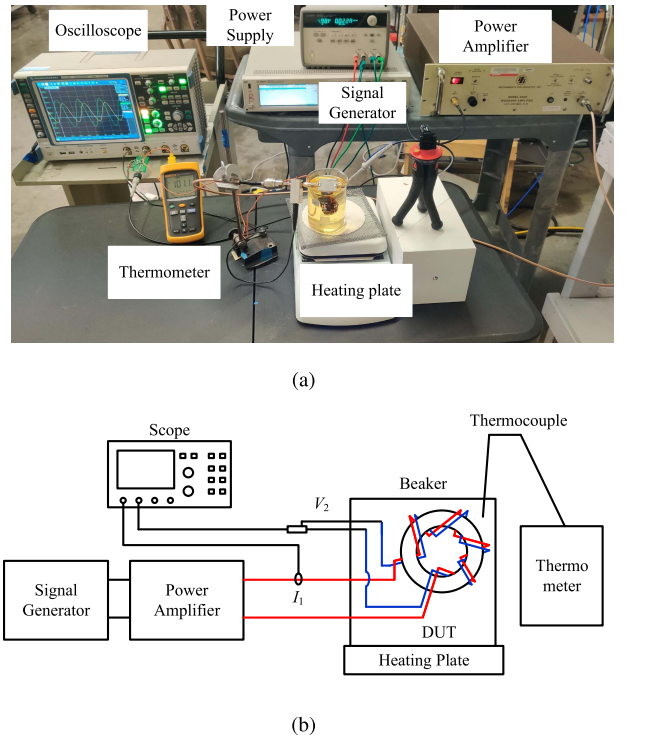

Fig. 13. (a) Photograph of the core characterization setup. (b) Diagram of the core loss measurement setup.

Fig. 14. Toroid samples with bifilar windings.

impedance is measured directly by the VNA according to [19]. The input impedance of the voltage probe decreases at a rate of 20 dB/dec, which validates the capacitor-based circuit model. In addition, the capacitances extracted from the measurement are 8.9, 3.6, and 2 pF when C_A is not added, while the expected capacitances are 10, 2.8, and 1 pF, respectively.

B. Current Probe Characterization

The current probe (Tektronix CT-2 with P6041 probe cable) and its transfer function are shown in Fig. 12. Two SMA connectors are connected in series and installed on the current probe so that the probe can be directly connected to other instruments using coaxial connectors. The current I_{IN} flowing through the probe can be measured by the output voltage V_{out}.

We note that the gain of the current probe is approximately a constant value up to 50 MHz, while the phase shift can reach 20° at 10 MHz. This phase shift is due to the propagation delay of the current probe and its cable.

V. Experimental Validation

A. Core Loss Characterization

To verify the proposed characterization method, an experiment was built, as shown in Fig. 13. It consists of a signal generator (Agilent N5181A), a power supply (Agilent E3648A), a power amplifier (Instruments for Industry 5500), and an oscilloscope (R&S RTO1024, 10 GS/s with a 2-GHz bandwidth). In addition, the ferrite core is immersed in the oil bath on a hot plate, and its temperature is supervised by a thermocouple. The setup supports high-temperature core loss measurement up to 100 °C without largely influencing the temperature of voltage and current probes. C_A is configured to be ∼1 pF to increase the input impedance of the voltage probe. We note that two capacitors (2.1 pF, Murata, dielectric: C0G, and voltage rating: 200 V) are connected in series to avoid capacitance variation due to the high voltage level.

Two different cores from TDK (R41.8/26.2/12.5N97) and Fair-Rite (T36/23/13-61) were characterized separately. Fig. 14 shows the CUT samples made with seven turns of AWG 24 copper wires. The losses measured by the in-house probe and P6251 (Tektronix, with a 1-in solder down tip) are compared. Both commercial and in-house probes are compensated for with the transfer functions measured by the VNA (Agilent E5071C).

1) Measurement Results for Fair-Rite 61: The measured core losses are compared with the datasheet results, as shown

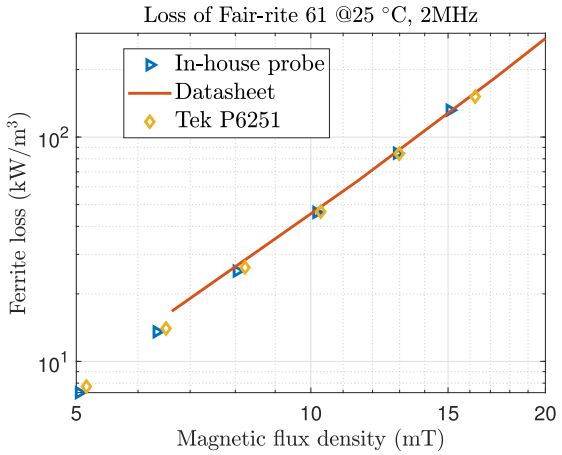

Fig. 15. Core loss comparison between the proposed method and the datasheet.

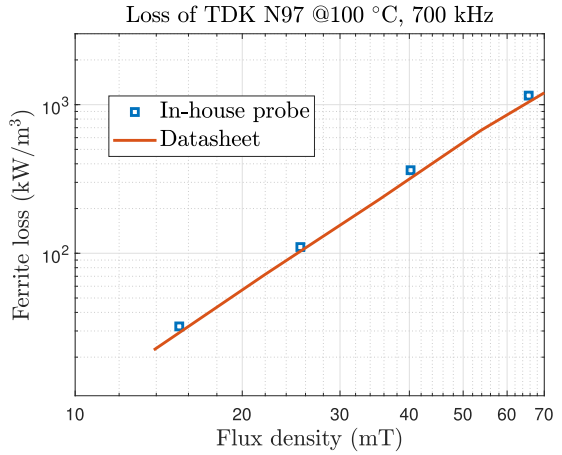

Fig. 16. Core loss comparison between the proposed method and the datasheet.

in Fig. 15. The excitation frequency was set to 2 MHz, and the core losses at 25 °C were measured. The losses measured by the in-house and the Tek P6251 are well matched, where the differences between the two probes are within 3%. In addition, the errors are within 8% if we assume that the manufacturer's loss measurement results are accurate. However, the loss due to mutual winding is not included and will be discussed in the next section.

2) Measurement Results for TDK® N97: To further demonstrate the measurement accuracy of the proposed method, the core loss of the TDK N97 core is measured at 100 °C with a 700-kHz excitation.

The measured core losses are compared with those given by the datasheet in Fig. 16. Similar to the previous measurement results, the discrepancy between the measurement results and the datasheet is less than 10%, which further validates the proposed probe characterization method.

B. Characterization of Mutual Impedance of a Three-Coil System

Due to the lack of a reference method for core loss characterization, validations performed with cores are not strong

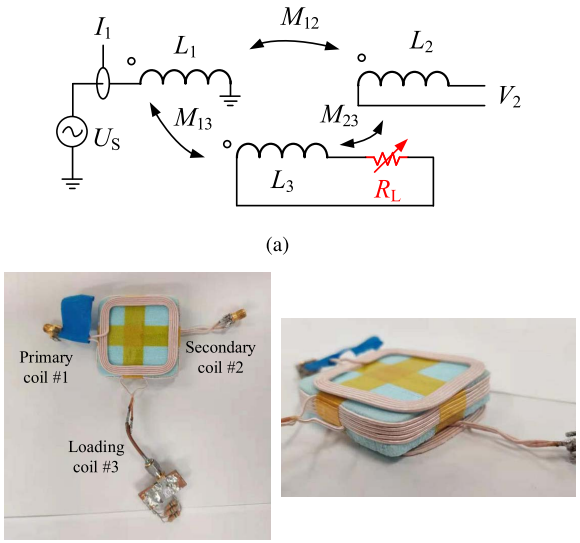

Fig. 17. (a) Equivalent circuit of the three-coil system. L_1, L_2, and L_3 correspond to self-inductances of the primary, secondary, and loading coils. M_{12}, M_{13}, and M_{22} represent the mutual inductances. R_L is the load resistance that is used to control the mutual impedance. (b) Three-coil system prototype.

supports for the proposed method. A three-coil system with an air core is then developed for further validation. The experimental setup is depicted in Fig. 17(a). The coil module consists of primary, secondary, and loading coils. According to Rezaei *et al.* [20], the mutual impedance Z_M between the primary and secondary coils can be expressed as

$$Z_M = \frac{V_2}{I_1} = \frac{\omega^2(M_{12}L_3 - M_{13}M_{23} - j\omega M_{12}R_L)}{R_L + j\omega L_3} \quad (17)$$

where V_2 is the open-circuit voltage of the secondary coil and I_1 is the input current of the primary coil. Due to the mutual coupling between three coils, Z_M can be controlled by the value of the load resistor R_L. We note that the three coils are assembled without a magnetic core, and Z_M is a constant value under different excitation levels. Therefore, Z_M measured by a VNA is compared with that measured by the setup shown in Fig. 13.

Fig. 18 compares the phases of Z_M measured by different instruments. The phase changes with the load resistance R_L, which validates the three-coil structure. In addition, the phase error between the two methods is limited to 0.2° in the frequency range of 2–15 MHz.

VI. Discussion

To ensure the accuracy of the proposed measurement method, it is necessary to identify and analyze various error sources in the system, including the influence of mutual resistance, measurement repeatability, loop size of the voltage probe, and linear region of probes.

A. Influence of Mutual Resistance

As discussed in [13] and [14], the mutual resistance between primary and secondary windings is another main error source

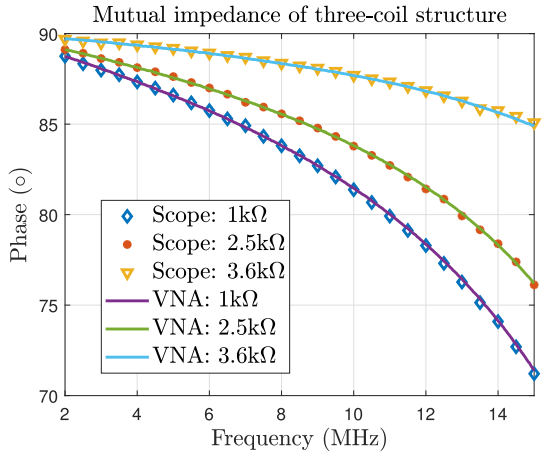

Fig. 18. Comparison of mutual impedance measured by VNA and scope under different loading resistances.

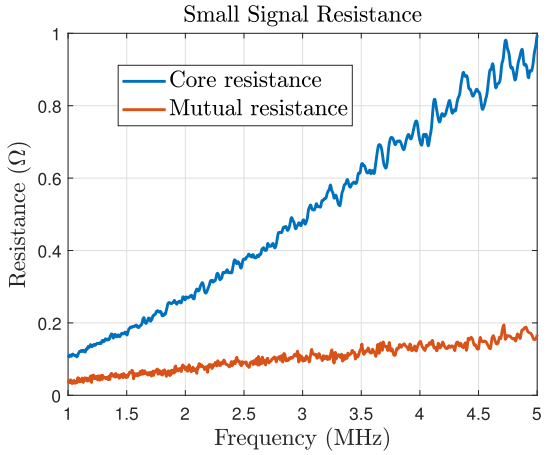

Fig. 19. Extracted small-signal core and mutual winding resistances. The output power of the VNA was configured as −10 dBm.

in core loss characterization. Unlike leakage winding loss, mutual resistance loss cannot be removed by the two-winding measurement method and, thus, can introduce significant error at high frequencies.

The small-signal core and mutual winding resistance of the Fair-Rite 61 sample are characterized by the VNA according to the measurement method proposed in [13], as shown in Fig. 19. The excitation current of VNA was configured as ∼2 mA, and the extracted mutual resistance was ∼75 mΩ at 2 MHz, which is much smaller than the equivalent core resistance. The mutual winding loss can be neglected.

B. Measurement Repeatability

The largest advantage of the proposed method is that the voltage and current probes are characterized before core loss measurement, and no tuning process is required during the test.

Repeatability of the measurement results is essential for the proposed method, as the positioning of the probes can potentially introduce uncertainty into the measurement results. Therefore, the results of ten measurements are shown

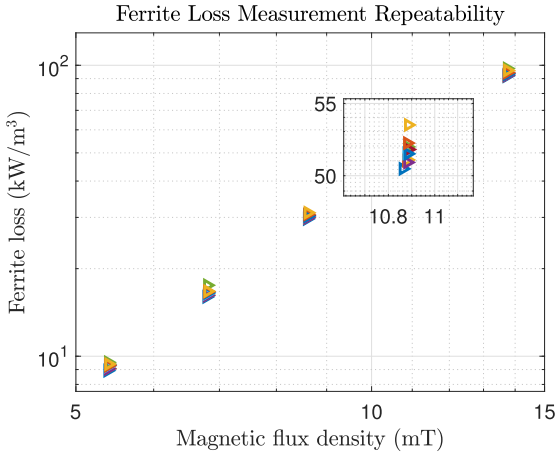

Fig. 20. Measurement repeatability of the proposed method.

Fig. 21. Photograph of different grounding structures.

in Fig. 20, where both the voltage and current probes are removed and reconnected to the circuit. The variation of the results is within 6%.

C. Error Caused by Loop Size of Pickup Structure

The input impedance of a voltage probe can be simplified as a capacitor as we demonstrated in Fig. 11. However, the parasitic inductance of the pickup structure, which comes from the probe and installation of the DUT, can introduce extra errors in the voltage measurement. To evaluate the error brought by the loop size, illustrated in Fig. 21, the differences in transfer functions measured with two ground structures are illustrated in Fig. 22. The comparison is performed without an external capacitor C_A, which is the case that can be most affected by the parasitic inductance.

Due to the larger loop size formed by the tip and 3-in ground lead, extra attenuation and phase delay are introduced. We note that the phase difference is limited to 0.1°, and the difference in gain is within 1% below 20 MHz. Despite that the error is almost negligible below 20 MHz, the consistency of the measurement loop between probe characterization and real measurement is still suggested to eliminate the possible error.

D. Linear Region of Probes

The saturation of both voltage probe and current probes should be avoided. The linear operating region of the voltage

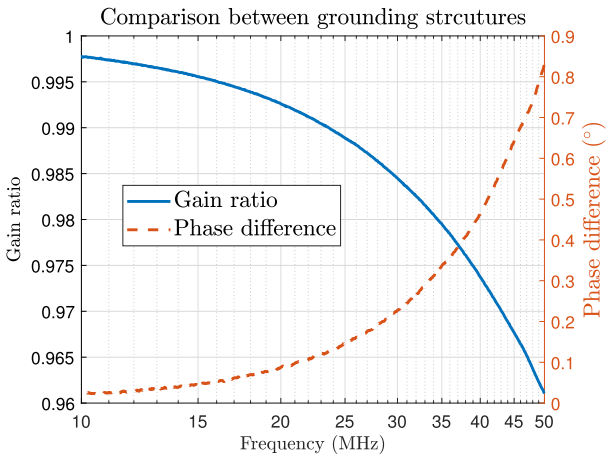

Fig. 22. Gain ratio and phase difference between the ground spring and the 3-in ground lead.

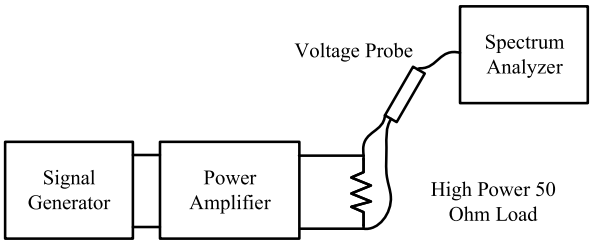

Fig. 23. Measurement setup for the voltage transfer curve of voltage probing system.

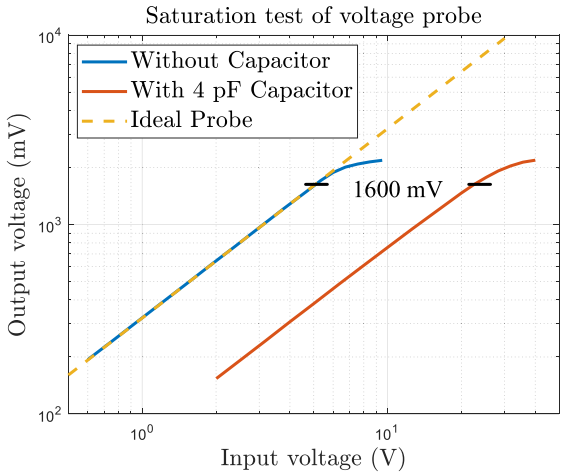

Fig. 24. Voltage transfer curve of the voltage probing system with different configurations.

probing system can be evaluated by the voltage transfer curve, which is defined as the ratio between input and output voltages. The same concept can be applied for the current probe or referring to the data from the manufacturer [21].

The output signal of the proposed voltage probing system is measured by a spectrum analyzer (R&S FSV30) under sinusoidal excitation, as shown in Fig. 23. The input voltage is controlled by the signal generator, and the frequency is configured as 2 MHz. We note that the input voltage is measured separately with a reference active voltage probe (Tektronix: P6251).

The measured voltage transfer curves of the in-house active probe are shown and plotted against an ideal one. As the gain of the internal amplifier is a constant value, the boundary compression point can be defined according to the output voltage. For this example, the probing system can be regarded as a linear system when the output voltage is less than 1.6 V, as shown in Fig. 24. In addition, the total harmonic distortion of the probing system can be limited to 1% when the output voltage is below the threshold voltage. In summary, a higher attenuation should be applied to the probe once its output voltage is larger than 1.6 V.

VII. Conclusion

This article proposes an impedance converter-based probe characterization method for core loss characterization. The in-house active probe eliminates the constraint of the complex probe-to-instrument interface in commercial probes, and the VNA-based probe characterization method can be applied. DUT-free probe compensation is then allowed without extra phase cancellation components, which enables a fast and accurate core loss characterization. The proposed method is experimentally validated by a linear three-coil system with controllable mutual impedance. It demonstrates that the error in phase is limited to 0.2° compared with a VNA below 15 MHz. In addition, the core loss error between measurement results and data from the datasheet is below 10%.

Possible sources of error using this method are analyzed. In particular, the linear operating regions of probes are evaluated, which overcomes the limitation of the small-signal measurement of a VNA.

References

[1] M. Araghchini *et al.*, "Modeling and measured verification of stored energy and loss in MEMS toroidal inductors," *IEEE Trans. Ind. Appl.*, vol. 50, no. 3, pp. 2029–2038, Nov. 2014.

[2] C. R. Sullivan, B. A. Reese, A. L. F. Stein, and P. A. Kyaw, "On size and magnetics: Why small efficient power inductors are rare," in *Proc. Int. Symp. 3D Power Electron. Integr. Manuf. (3D-PEIM)*, Jun. 2016, pp. 1–23.

[3] J. Qiu and C. R. Sullivan, "Radial-anisotropy thin-film magnetic material for high-power-density toroidal inductors netic material 3 small radial-anisotropy magnetic toroidal cores for inductors with high power density," in *Proc. 7th Int. Conf. Integr. Power Electron. Syst. (CIPS)*, Mar. 2012, pp. 1–6.

[4] V. C. Valchev and A. Van den Bossche, *Inductors and Transformers for Power Electronics*. Boca Raton, FL, USA: CRC Press, 2018.

[5] Y. Yan, K. D. T. Ngo, D. Hou, M. Mu, Y. Mei, and G.-Q. Lu, "Effect of sintering temperature on magnetic core-loss properties of a NiCuZn ferrite for high-frequency power converters," *J. Electron. Mater.*, vol. 44, no. 10, pp. 3788–3794, Oct. 2015.

[6] A. Van Den Bossche, V. C. Valchev, and G. B. Georgiev, "Measurement and loss model of ferrites with non-sinusoidal waveforms," in *Proc. IEEE 35th Annu. Power Electron. Spec. Conf. (PESC)*, vol. 6, no. 1, Jun. 2004, pp. 4814–4818.

[7] C. A. Baguley, B. Carsten, and U. K. Madawala, "An investigation into the impact of DC bias conditions on ferrite core losses," in *Proc. 33rd Annu. Conf. IEEE Ind. Electron. Soc. (IECON)*, vol. 44, no. 2, Nov. 2007, pp. 1408–1413.

[8] J. Mühlethale, J. Biela, J. W. Kolar, and A. Ecklebe, "Core losses under the DC bias condition based on Steinmetz parameters," *IEEE Trans. Power Electron.*, vol. 27, no. 2, pp. 953–963, Feb. 2012.

[9] V. J. Thottuvelil, T. G. Wilson, and H. A. Owen, "High-frequency measurement techniques for magnetic cores," in *Proc. IEEE Power Electron. Spec. Conf.*, Jun. 1985, pp. 41–53.

[10] M. Mu, Q. Li, D. J. Gilham, F. C. Lee, and K. D. T. Ngo, "New core loss measurement method for high-frequency magnetic materials," *IEEE Trans. Power Electron.*, vol. 29, no. 8, pp. 4374–4381, Aug. 2014.
[11] D. Hou, M. Mu, F. C. Lee, and Q. Li, "New high-frequency core loss measurement method with partial cancellation concept," *IEEE Trans. Power Electron.*, vol. 32, no. 4, pp. 2987–2994, Apr. 2017.
[12] S. Prabhakaran and C. R. Sullivan, "Impedance-analyzer measurements of high-frequency power passives: Techniques for high power and low impedance," in *Proc. Conf. Rec. IEEE Ind. Appl. Conf. 37th IAS Annu. Meeting*, vol. 2, Oct. 2002, pp. 1360–1367.
[13] B. X. Foo, A. L. F. Stein, and C. R. Sullivan, "A step-by-step guide to extracting winding resistance from an impedance measurement," in *Proc. IEEE Appl. Power Electron. Conf. Expo. (APEC)*, Mar. 2017, pp. 861–867.
[14] K. Niyomsatian, J. J. C. Gyselinck, and R. V. Sabariego, "Experimental extraction of winding resistance in litz-wire transformers—Influence of winding mutual resistance," *IEEE Trans. Power Electron.*, vol. 34, no. 7, pp. 6736–6746, Jul. 2018.
[15] C. Fernandez, Z. Pavlovic, S. Kulkarni, P. McCloskey, and C. O'Mathuna, "Novel high-frequency electrical characterization technique for magnetic passive devices," *IEEE J. Emerg. Sel. Topics Power Electron.*, vol. 6, no. 2, pp. 621–628, Jun. 2018.
[16] *P6250 and P6251 Quick Start User Manual*. [Online]. Available: https://www.tek.com/probes-and-accessories/high-voltage-differential-probes-manual
[17] *6 Hints for Better Scope Probing*. [Online]. Available: https://www.keysight.com/upload/cmcupload/All/Probing-6-Hints-Scopes-Dec12-2007-webcast.pdf
[18] G. Cerri, R. De Leo, V. M. Primiani, S. Pennesi, and P. Russo, "Wideband characterization of current probes," *IEEE Trans. Electromagn. Compat.*, vol. 45, no. 4, pp. 616–625, Nov. 2003.
[19] *Ultra-Low Impedance Measurements Using 2-Port Measurements*. [Online]. Available: https://www.keysight.com/us/en/assets/7018-08474/application-notes/5989-5935.pdf
[20] H. Rezaei, V. Khilkevich, S. Yong, D. S. Stutts, and D. Pommerenke, "Mechanical magnetic field generator for communication in the ULF range," *IEEE Trans. Antennas Propag.*, vol. 68, no. 3, pp. 2332–2339, Nov. 2020.
[21] *Ct-1 and Ct-2 Current Transformer Instructions*. [Online]. Available: https://download.tek.com/manual/070795702web.pdf

Anfeng Huang (Student Member, IEEE) was born in Guangxi, China, in July 1992. He received the B.E. and M.S. degrees from Xidian University, Xi'an, Shaanxi, China, in 2014 and 2017, respectively. He is currently pursuing the Ph.D. degree in electrical engineering with the electromagnetic compatibility (EMC) Laboratory, Missouri University of Science and Technology, Rolla, MO, USA.

His current research interests include electromagnetic interference (EMI) in power electronics, magnetic material characterization, and low-level signal measurement.

Hongseok Kim (Member, IEEE) received the Ph.D. degree in electrical engineering (future vehicle) from the Korea Advanced Institute of Science and Technology (KAIST), Daejeon, South Korea, in 2017.

He is currently an Assistant Research Professor with the electromagnetic compatibility (EMC) Laboratory, Missouri University of Science and Technology, Rolla, MO, USA. His research fields are EMC modeling, analysis, and design of automotive power systems, including dc–dc converters, resonant converters, high/low-power wireless chargers, and high-/low-voltage motor drive systems.

Hanyu Zhang received the B.E. and M.S. degrees in electrical engineering from the Southwest University of Science and Technology, Mianyang, China, in 2017 and 2020, respectively. He is currently pursuing the Ph.D. degree in electrical engineering with the electromagnetic compatibility (EMC) Laboratory, Missouri University of Science and Technology, Rolla, MO, USA.

His research interests include power electronics and wireless power transfer.

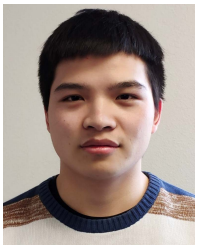

Qiusen He received the B.E. and M.S. degrees in electrical engineering from the Southwest University of Science and Technology, Mianyang, China, in 2017 and 2020, respectively.

He was an Intern Student with the electromagnetic compatibility (EMC) Laboratory, Missouri University of Science and Technology (Missouri S&T), Rolla, MO, USA. His current research interests include wireless power transfer for EV and MOSFET gate driver design.

David Pommerenke (Fellow, IEEE) received the Diploma and Ph.D. degrees in electrical engineering from Technical University Berlin, Berlin, Germany, in 1989 and 1995, respectively.

After working at Hewlett Packard for five years, he joined the electromagnetic compatibility (EMC) Laboratory, Missouri University of Science and Technology (S&T), Rolla, MO, USA, in 2001. In 2020, he moved to Graz, Austria, to join the Graz EMC Lab, Graz University of Technology, Graz. He has published more than 150 journal articles. He is an inventor of 13 patents. His research interests include EMC, electrostatic discharge (ESD), electronics, numerical simulations, measurement methods, and instrumentations.

Dr. Pommerenke is also an Associate Editor of the IEEE TRANSACTIONS ON ELECTROMAGNETIC COMPATIBILITY (TEMC).

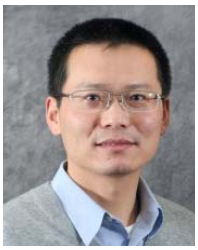

Jun Fan (Fellow, IEEE) received the B.S. and M.S. degrees in electrical engineering from Tsinghua University, Beijing, China, in 1994 and 1997, respectively, and the Ph.D. degree in electrical engineering from the University of Missouri–Rolla, Rolla, MO, USA, in 2000.

From 2000 to 2007, he was a Consultant Engineer with NCR Corporation, San Diego, CA, USA. In July 2007, he joined the Missouri University of Science and Technology (formerly the University of Missouri–Rolla), where he is currently an Associate Professor with the Missouri S&T electromagnetic compatibility (EMC) Laboratory. His current research interests include signal integrity and electromagnetic interference (EMI) designs in high-speed digital systems, dc power-bus modeling, intersystem EMI and radio frequency interference, printed circuit board noise reduction, differential signaling, and cable/connector designs.

Dr. Fan received the IEEE EMC Society Technical Achievement Award in August 2009. He was the Chair of the IEEE EMC Society's TC-9 Computational Electromagnetics Committee from 2006 to 2008 and a Distinguished Lecturer of the IEEE EMC Society from 2007 to 2008. He is also the Vice-Chair of the Technical Advisory Committee of the IEEE EMC Society. He is also an Associate Editor of the IEEE TRANSACTIONS ON ELECTROMAGNETIC COMPATIBILITY (TEMC) and the *EMC Magazine*.